

The E_p -Flux Correlation in the Rising and Decaying Phases of Gamma-Ray Burst Pulses: Evidence for Viewing Angle Effect?

R.-J. Lu¹, S.-J. Hou¹ and En-Wei Liang^{1,2}
luruijing@gxu.edu.cn; lew@gxu.edu.cn

ABSTRACT

A time-resolved spectral analysis for a sample of 22 intense, broad GRB pulses from the *CGRO/BATSE* GRB sample is presented. We fit the spectra with the Band function and investigate the correlation between the observed flux (F) and the peak energy (E_p) of the νf_ν spectrum in the rising and decaying phases of these pulses. Two kinds of E_p evolution trends, i.e., hard-to-soft (the two-third pulses in our sample) and E_p -tracing- F (the one-third pulses in our sample) are observed in pulses from different GRBs and even from different pulses of the same burst. No dependence of spectral evolution feature on the pulse shape is found. A tight $F - E_p$ positive correlation is observed in the decaying phases, with a power-law index ~ 2.2 , which is much shallower than that expectation of the curvature effect. In the rising phase, the observed F is either correlated or anti-correlated with E_p , depending on the spectral evolution feature, and the power-law index of the correlation is dramatically different among pulses. More than 80% of the low energy photon indices in the time-resolved spectra whose E_p is anti-correlated with F during the rising phase violate the death line of the synchrotron radiation, disfavoring the synchrotron radiation model for these gamma-rays. The $F - E_p$ correlation, especially for those GRBs with E_p -tracking- F spectral evolution, may be due to the viewing angle and jet structure effects. In this scenario, the observed $F - E_p$ correlation in the rising phase may be due to the line of sight from off-beam to on-beam toward a structured jet (or jitter), and the decaying phase is contributed by both the on-beam emission and the decayed photons from high latitude of the GRB fireball, resulting in a shallower slope of the observed $F - E_p$ correlation than that predicted by the pure curvature effect.

Subject headings: gamma-ray burst: general—radiation mechanisms: non-thermal—methods: data analysis

1. Introduction

The physics of prompt emission of gamma-ray bursts (GRBs) remains as a great puzzle. Analysis for a large sample of GRB spectra observed with Burst and Transient Source Experiment (BATSE) on board *CGRO* reveals that the GRB spectra are non-thermal, well-fit with a smoothly-jointed broken power-law, the so-called Band function (Band et al. 1993). The physical radiation mechanism

that shapes such a spectrum shape is unclear (e.g., Zhang & Mészáros et al. 2004). The peak energy of the νf_ν spectrum (E_p) is one of the most interesting parameters of GRBs. The relation between the burst energy and E_p may shed light on the physics of GRBs (Zhang & Mészáros 2002). With a sample of 12 GRBs detected by BeppoSAX, Amati et al. (2002) found a positive correlation between the isotropic gamma-ray energy (E_{iso}) and the peak energy in the burst frame ($E_{p,z}$). This correlation was confirmed and even extended to the X-ray flashes by the observations with *HETE-2* and *Swift* (Sakamoto et al., 2006; Amati 2006). By geometrical-correction for the jet beaming ef-

¹Department of Physics, Guangxi University, Guangxi 530004, China.

²Department of Physics and Astronomy, University of Nevada Las Vegas, Las Vegas, NV 89154, USA.

fect or empirically incorporating the breaks in the optical afterglow lightcurves, this correlation is even getting tighter (Ghirlanda et al. 2004; Liang & Zhang 2005). Similarly, the isotropic peak luminosity (L_p) is correlated with $E_{p,z}$ (Wei et al. 2003; Yonetoku et al. 2004). The average flux (F) in a given epoch is also correlated with the E_p in the corresponding epoch within a GRB (Liang et al. 2004). The $F - E_p$ correlation suggests that the $E_p - E_{\text{iso}}$ and the $E_p - L_p$ correlations would not be due to the observational selection effects (c.f., Nakar & Piran 2005; Band & Preece 2005; Shahmoradi & Nemiroff 2009). All the prompt GRB emission models predict E_p as a function of both E_{iso} (or L_p) and the initial Lorentz factor of the GRB fireball (Γ_0) (e.g. Table 1 of Zhang & Mészáros 2002). Most recently, Liang et al. (2010) discover a tight correlation between E_{iso} and Γ_0 , i.e., $\Gamma_0 = 182(E_{\text{iso}}/10^{52} \text{ erg})^{0.25}$. This correlation poses constraints on prompt emission models. For example, the internal shock synchrotron model, the most favorite model for GRBs, predicts $E_p \propto L^{1/2}\Gamma_0^{-2}$ (Zhang & Mészáros 2002). Combining with the trivial proportionality of $L \propto E_{\text{iso}}$, one can find that E_p should not depend on L , indicating that the $E_p - E_{\text{iso}}$ correlation may not be explained in the framework of the internal shock synchrotron model.

This paper dedicates to revisit the $F - E_p$ correlation and its possible physical origin. The E_p of a given burst evolves with time, tracing with the lightcurve (E_p -tracing- F) or evolving as hard-to-soft (Liang & Kargatis 1996; Ford et al. 1995; Kaneko et al. 2006). Intuitively, the $F - E_p$ correlation should be the foundation of the Amati relation, if both are based on the same physical origin. Since those GRBs having hard-to-soft spectral evolution do not have a coherent $F - E_p$ correlation, they should violate the Amati relation. However, the current sample of GRBs with both E_{iso} and E_p measurements well follow the Amati-relation (Amati et al. 2009), regardless of the spectral evolution feature of these GRBs. For example, although the spectrum of GRB 060218 evolves as hard-to-soft (Toma et al. 2007; Dong et al. 2010), it well satisfies the Amati-relation (Amati et al. 2006). Therefore, the Amati relation seems to be unrelated to the dependence of F on E_p . This gives rise to a big puzzle of the physical origin of the Amati-relation.

It is well known that the GRB lightcurves are generally composed of some overlapped pulses. An individual shock episode may give rise to a pulse, and the random superposition of many such pulses results in the observed complexity of GRB light curves. As the building blocks of GRB lightcurves, the broad, well-separated pulses are good candidates to reveal the physics of GRBs. The E_p evolution within GRB pulses has been extensively studied, especially for the decaying phase of pulses (Golenetskii et al. 1983; Norris et al. 1986; Kargatis et al. 1994, 1995; Bhat et al. 1994; Crider et al. 1999; Peng et al. 2009; Lu & Liang 2010). While the decaying phase of a GRB pulse might be contributed by the curvature effect of the GRB fireball (e.g., Fenimore et al. 1995; Kobayashi et al. 1997; Qin et al. 2002; Dermer 2004; Shen et al. 2005), both the temporal and spectral behaviors of the rise phase of a pulse may depend on the dynamics of the GRB fireball, the electron acceleration, and the radiation mechanism (e.g., Kobayashi et al. 1997). The $F - E_p$ correlations in the two phases, if any, should dramatically different, which was shown by Ohno et al. 2009 and Ghirlanda et al. (2010) for some bright GRBs. We here present a detailed analysis on the $F - E_p$ relation in both the rising and decaying phases of smooth, broad GRB pulses observed with *CGRO/BATSE*.

We present our sample and spectral analysis in Section 2. The lightcurves and the E_p evolution as well as the $F - E_p$ correlation are shown in Section 3. Since the low energy photon index of the Band function is critical to justify if the radiation is from synchrotron radiation, we present the distribution of the low energy photon indices for those spectra having an anti-correlation between E_p and F in Section 4. We discuss the possible physical origin of the $F - E_p$ correlation (or anti-correlation) in Section 5. Conclusions are presented in Section 6.

2. Sample selection and time-resolved spectral analysis

We make use the data observed with BATSE¹. Kaneko et al. (2006) presented a sample of 8459 time-resolved burst spectra for 350 bright GRBs observed with BATSE. Our sample of GRB pulses are taken from this sample. We download the spectra data from the web site <http://www.batse.msfc.nasa.gov/~kaneko/>. We first select bright pulses from the lightcurves of these GRBs. Technically, it is difficult to define a genuine pulse from GRB lightcurves. Flickering and/or superimposing weak pulses make complication to employ a rigid criterion to select our pulse sample. We use the same criteria as that described in Liang et al. (2002) to select our sample. We make time-resolved analysis for these pulses with RMFIT, a package of spectral analysis routines (version 3.3) developed by the BATSE team (Mallozzi et al. 2005 and Preece et al. 2008). Although the time-resolved spectral analysis for these pulses are present in Kaneko et al. (2006), we re-do the time-resolved spectral analysis for these spectra by lowering down a little bit of the signal-to-noise ratio (SNR) in each time slice in order to get more slices in both the rising and decaying phases for our analysis. We adopt $SNR = 30$, compared to $SNR = 45$ in Kaneko et al. (2006). We fit the spectra with the Band function (Band et al. 1993). The reduced χ^2 of our fits are normally $\sim 0.9 - 1.1$. Since we focus on the $F - E_p$ correlation in both the rising and decaying parts of a pulse, our sample includes only those pulses that are intense and broad enough to make robust spectral fit for at least three time slices in the rising and decaying segments, respectively. We finally get a sample of 22 pulses. The average flux F in each time slide is then derived from the Band model spectral parameters in the 30-10⁴ keV band (as done in Yonetoku et al. 2004 and Liang et al. 2004). Our time-resolved spectral analysis results are available in the online material of this paper.

¹Although *Fermi*/GBM has established a large sample of GRBs in similar energy band as *CGRO*/BATSE, we only use the data observed with BATSE in this analysis since they are well-studied and the uncertainty of background subtraction for GBM data make our time-resolved spectral fits has larger uncertainty than BATSE data (especially in the rising phases).

3. Temporal evolution of E_p and $F - E_p$ correlation

Figure 1 shows the lightcurve with temporal evolution of the E_p and the $F - E_p$ correlation for the pulses in our sample. It is found that the shape of these pulses are semi-symmetric, slightly different from the FRED pulses usually seen in the GRB lightcurves. This would be due to our sample selection effect since we include only those pulses that the rising part is long and bright enough to make time-resolved spectral fit.

The spectral evolution feature is well classified into two groups, i.e., hard-to-soft and E_p -tracing- F . Fifteen out of the 22 belong to the group of the hard-to-soft evolution, including # 647, 973, 1883, 2083, 2193, 2387, 3658, 5478, 6397, 6504, 6630, 7293, 7475, 7588, and 7771. The others, including #1625, 1733, 1956, 3003, 3765, 5523 and 5601, are of the E_p -tracing-flux group. No dependence of the spectral evolution feature on the pulse shape is found.

The observed fluxes in the decaying phases of these pulses are tightly correlated with E_p . We fit the $F - E_p$ correlation (or anti-correlation) in the rising and decaying parts with a power-law model $F \propto E_p^{\kappa_r(\kappa_d)}$, where $\kappa_r(\kappa_d)$ is the power-law index in the rising (decaying) part. The results are reported in Table 1. As shown in Figure 1, although no universal κ_d value is found about pulses, the distribution of κ_d clustered at ~ 2.20 (see also Borgonovo & Ryde 2001). We should emphasize that the large dispersion of κ_d is not due to the uncertainty of κ_d measurement. As shown in Table 1, even considering the the errors of κ_d , the κ_d of some pulses confidently deviates ~ 2 . The dispersion of κ_d would be physical (see discussion below). The observed flux in the rising phase are either correlated or anti-correlated with E_p in the rising phase, depending on the spectral evolution feature. The power-law index in the $F - E_p$ correlation in the rising phase, κ_r , spans from -4 to 10 without any correlation with the pulse shape and κ_d .

It is also very interesting that the E_p evolution in different pulses of a GRB may be also different. Two well-separated pulses are observed in the BATSE trigger# 2038. As shown in Figure 2, the E_p evolves as hard-to-soft during the first pulse but it traces the intensity of the flux in the second

pulse. The $F - E_p$ correlations in the decaying phases of the two pulses are similar. However, they are absolutely different in the rising phases.

4. Distributions of low-energy photon indices

The $F - E_p$ anti-correlation observed in GRB pulses having a hard-to-soft spectral evolution is inconsistent with the expectation of the most favorite GRB model, the synchrotron internal shock model. The model predicts that the low-energy photon index should not exceed $-2/3$, with the assumption that the optical depth of the shocked material is less than unity (e.g., Preece et al. 1998). We show the distribution of the best fit α for those time-resolved spectra whose E_p is anti-correlated with F in Figure 3. It is found that 50 out of the 61 spectra ($\sim 82\%$) have a low energy photon index being larger than $-2/3$. This percentage is only 32% for those spectra whose E_p is positively correlation with F . If taking the values of their 1σ lower limits, we find the two percentages become $\sim 78\%$ and $\sim 19\%$, respectively. Therefore, the $F - E_p$ anti-correlation cannot be explained with the synchrotron radiation model.

5. Implications

5.1. E_p evolution confronting with the radiation models

The E_p evolution feature within a pulse is essential to study radiation models of the prompt emission. As shown above, the most common spectral evolution feature in GRB pulses (the two-third pulses in our sample) is the hard-to-soft evolution, in which the peak energy of the spectrum decreases monotonically over the entire pulse (Norris et al. 1986), and the secondly one (the one-third of the pulses in our sample) is the E_p -tracking- F (Golenetskii et al. 1983). More interestingly, the E_p in different pulses of # 2083 even shows different evolution behavior (see Figure 2). Different models may design some kinds of E_p evolution. However, it is difficult to accommodate two completely different evolution trends under one mechanism.

The most favorite GRB model is the synchrotron internal shock model. In this model, a GRB pulse is produced by the collision of two

relativistic shells, in which the rising phase is related to the dynamics and the physical parameters of the shocked fireball shell and the decay phase is due to the time decay of photons from the high latitude of the fireball, the so-called curvature effect (e.g., Kobayashi et al. 1997). Most recently, Zhang & Yan (2010, in preparation) proposed that the internal collision may induce magnetic reconnection and turbulence to explain the prompt gamma-ray emission. In their model it is expected that E_p is positively related to σ , the ratio between Poynting flux and baryonic flux. Since the magnetic energy is continuously converted to the particle energy during an emission episode, the hard-to-soft E_p evolution is naturally expected from their model.

The radiation models discussed above essentially explain the hard-to-soft emission with the decrease of the energy of radiating particles over the emission episode. The E_p -tracking- F evolution, however, is hard to interpret with these models, especially for different E_p evolution features observed among pulses of a given GRB as shown in Figure 2 and the observed $F - E_p$ anti-correlation. The α of more than 80% time-resolved spectra whose E_p are anti-correlated with F violate the death line of the synchrotron radiation model.

5.2. $F - E_p$ correlation confronting with viewing angle effect

It is most likely that the E_p evolution and the $F - E_p$ correlation are not related to radiation physics. It was also proposed that the broad pulses in GRBs may be shaped by GRB jet precession (Portegies Zwart et al. 1999; Reynoso et al. 2006; Lei et al. 2007; Liu et al. 2010). The waggle of the GRB jet may result in off-beam and on-beam cycle to produce broad pulses ² and the E_p -tracking- F spectral evolution (Liu et al. 2010). The observed lightcurve for initial off-beam to on-beam may rise rapidly to trigger our detectors, especially in the case of a sharp-edge, highly structured jet (Panaitescu et al. 1998; Panaitescu & Vestrand 2008), shaping a fast-rise-exponential-decay pulse and hard-to-soft spectral evolution since the early rising part may be not bright enough to trigger our instruments. This may explain the observed

²It was suggested that the micro-variability in the GRB pulses are attributed to the turbulence of blast wave (Zhang & Yan 2010, in preparation)

different spectral evolution trends in the pulses of a burst as shown in Figure 2.

A clear anti-correlation between F and E_p is observed in the rising phase of a pulse with hard-to-soft spectral evolution, but the power-law index of the correlation is dramatically different among pulses, indicating that no universal relation is observed. This may be reasonable since the emission in the rising phase may be complicated by the dynamics of the fireball, the radiation mechanisms, the jet structure and viewing angle, micro physical parameters, etc. However, one is difficult to expect a clear $F - E_p$ correlation from stochastic dynamics of the fireball and particle acceleration process (e.g., Zhang & Mészáro 2002). Therefore, the $F - E_p$ correlation observed in a given pulse, especially for those GRBs with E_p -tracking- F spectral evolution, may be due to the viewing angle and jet structure effects, as we discuss above.

In the viewing angle and jet structure dominated scenario, the contribution of the high latitude photons from the fireball (the so-called curvature effect) would be increased in the decaying phase of a pulse and it should dominate the observed flux when the line of sight moves out the jet edge. Therefore, the mix of the on-axis and off-axis contributions may result in a shallower decay slope of the observed $F - E_p$ correlation as theoretical prediction. If the curvature effect dominates the decaying phase of the pulses, the expected $F - E_p$ relation at late time should be $F \propto E_p^3$ (e.g., Fenimore et al. 1995; Kumar & Panaiteescu 2000; Dermer et al. 2004). As shown in Fig. 1, the κ_d of most GRBs in our sample are indeed shallower than the prediction³.

The α distribution may shed light on the jet structure and radiation physics. Medvedev (2006) showed that spectrum of jitter radiation from GRB shocks containing small-scale magnetic fields and propagating at an angle with respect to the line of sight may vary considerably. The low-energy photon index may be significantly larger than the death line of the synchrotron radiation, i.e., $-2/3$. The E_p evolution and $F - E_p$ correlation may be explained with a combined effect of tempo-

³As shown by Zhang et al. (2009), the curvature effect involving a non-power-law spectrum in the radiating surface also modify the slope of the $F - E_p$ correlation(see also Qin 2008)

ral variation of the viewing angle and relativistic aberration of an individual thin, instantaneously illuminated shell.

5.3. $F - E_p$ correlation vs the Amati relation

The correlation between the observed flux and E_p within a GRB pulse is critical to explore the physics of the observed $L - E_p$ and $E_{iso} - E_p$ relations (Amati et al. 2002; Liang et al. 2004). The $L - E_p$ and $E_{iso} - E_p$ relations would globally reflect the $F - E_p$ correlation within a GRB. Essentially, they are time-integrated effect of the $F - E_p$ correlation (Firmani et al. 2009). Although the distribution of κ_d for the pulses in our sample has large dispersion, it normally peaks at 2. The emission in the decaying phases of all pulses in a GRB should dominate the total emission of the burst since the duration of the decaying phase of a pulse is generally much longer than the rising phase. Therefore, one may observe an $F - E_p$ correlation within a GRB or an $E_{iso} - E_p$ correlation among bursts, with a power-law index ~ 2 . We illustrate the $F - E_p$ correlation within a GRB with multiple pulse in Figure 4. An $F - E_p$ correlation with a power-law index ~ 2 is clearly seen. Therefore, the $L_p - E_p$ or $E_{iso} - E_p$ correlations should be dominated by the $F - E_p$ correlation. As discussed above, the $F - E_p$ is difficult to explain with the radiation physics. The $L_p - E_p$ and $E_{iso} - E_p$ correlations thus may not be interpreted with the radiation models. This is consistent with that inferred from the recent discovery of the tight correlation between the E_{iso} and the initial Lorentz factors of the GRB fireball (Liang et al. 2010).

6. Conclusions

With our time-resolved spectral analysis for a sample of 22 intense, broad GRB pulses we find that the E_p evolution feature is well classified into two groups, i.e., hard-to-soft (two-third pulses in our sample) and E_p tracing- F (one-third pulses in our sample). Two kinds of spectral evolutionary trends are also observed in different pulses of a burst. No dependence of spectral evolution feature on the pulse shape is observed.

A tight $F - E_p$ correlation, $F \propto E^{\kappa_d}$, is observed in the decaying phases of these pulse. Although the κ_d ranges in a broad range, from 0.6

to ~ 4.0 , their distribution normally peaks at ~ 2 , much shallower than that expectation of the curvature effect. In the rising phase, the observed F is either correlated or anti-correlated with E_p , $F \propto E_p^{\kappa_r}$, depending on the spectral evolution feature. The distribution of κ_r spans from -4 to 10 without any correlation with the pulse shape and κ_d . More than 80% of the low energy photon indices in the time-resolved spectra whose E_p is anti-correlated with F violate the death line of the synchrotron radiation.

The spectral evolution features and the observed $F - E_p$ correlation are difficult to explain with the radiation models. We propose that the observed the $F-E_p$ correlation observed in a given pulse, especially for those GRBs with E_p -tracking- F spectral evolution, may be due to the viewing angle and jet structure effects. In this scenario, the observed $F - E_p$ correlation in the rising phase is due to the line of sight from off-beam to on-beam toward a structured jet. The contribution of the high latitude photons from the fireball(the so-called curvature effect) would be increased in the decaying phase of a pulse and it should dominate the observed flux when the line of sight moves out the jet edge. Therefore, the mixed contributions from the on-beam and the curvature effect may result in a shallower decay slope of the observed $F - E_p$ correlation as theoretical prediction.

We appreciate valuable suggestions from the referee. We also thank Bing Zhang & Yi-Ping Qin for helpful discussion. This work is supported by the National Natural Science Foundation of China under grants No. 10747001 and 10873002, National Basic Research Program ("973" Program) of China (Grant 2009CB824800), Chinese Academy of Science (under grant KJCXZ-YWT19), Guangxi SHI-BAI-QIAN project (Grant 2007201), Guangxi Science Foundation (2010GXNSFA013112 and 2010GXNSFC013011), the program for 100 Young and Middle-aged Disciplinary Leaders in Guangxi Higher Education Institutions, and the research foundation of Guangxi University (M30520). EWL is a visiting scholar of UNLV during the revision of this paper with support from NASA NNX09AT66G, NNX10AD48G, and NSF AST-0908362.

REFERENCES

- Amati, L., Frontera, F., & Guidorzi, C. 2009, A&A, 508, 173
- Amati, L., et al. 2002, A&A, 390, 81
- Amati, L. 2006, MNRAS, 372, 233
- Band, D., et al. 1993, ApJ, 413, 281
- Band, D. L., & Preece, R. D. 2005, ApJ, 627, 319
- Bhat, P. N., Fishman, G. J., Meegan, C. A., Wilson, R. B., Kouveliotou, C., Paciesas, W. S., Pendleton, G. N., & Schaefer, B. E. 1994, ApJ, 426, 604
- Borgonovo, L., & Ryde, F. 2001, ApJ, 548, 770
- Crider, A., Liang, E. P., Preece, R. D., Briggs, M. S., Pendleton, G. N., Paciesas, W. S., Band, D. L., & Matteson, J. L. 1999, A&AS, 138, 401
- Dermer, C. D. 2004, ApJ, 614, 284
- Dong, W., Liang, E. W., Lu, R. J., Science China G, 2010, 53 (S1), 78
- Fenimore, E. E., in 't Zand, J. J. M., Norris, J. P., Bonnell, J. T., & Nemiroff, R. J. 1995, ApJ, 448, L101
- Firmani, C., Cabrera, J. I., Avila-Reese, V., Ghisellini, G., Ghirlanda, G., Nava, L., & Bosnjak, Z. 2009, MNRAS, 393, 1209
- Ford, L. A., et al. 1995, ApJ, 439, 307
- Ghirlanda, G., Ghisellini, G., Firmani, C., Celotti, A., & Bosnjak, Z. 2005, MNRAS, 360, L45
- Ghirlanda, G., Nava, L., & Ghisellini, G. 2010, A&A, 511, A43
- Ghirlanda, G., Ghisellini, G., & Firmani, C. 2005, MNRAS, 361, L10
- Ghirlanda, G., Ghisellini, G., & Lazzati, D. 2004, ApJ, 616, 331
- Golenetskii, S. V., Mazets, E. P., Aptekar, R. L., & Ilinskii, V. N. 1983, Nature, 306, 451
- Kaneko, Y., Preece, R. D., Briggs, M. S., Paciesas, W. S., Meegan, C. A., & Band, D. L. 2006, ApJS, 166, 298

- Kargatis, V. E., Liang, E. P., Hurley, K. C., Barat, C., Eveno, E., & Niel, M. 1994, ApJ, 422, 260
- Kobayashi, S., Piran, T., & Sari, R. 1997, ApJ, 490, 92
- Lei, W. H., Wang, D. X., Gong, B. P., & Huang, C. Y. 2007, A&A, 468, 563
- Liang, E. W., Dai, Z. G., & Wu, X. F. 2004, ApJ, 606, L29
- Liang, E., & Kargatis, V. 1996, Nature, 381, 49
- Liang, E.-W., Xie, G.-Z., & Su, C.-Y. 2002, PASJ, 54, 1
- Liang, E. W., & Zhang, B. 2005, ApJ, 633, 611
- Liang, E.-W., Yi, S.-X., Zhang, J., LV, H.-J., Zhang, B.-B., & Zhang, B. 2009, ApJ, submitted (arXiv:0912.4800).
- Liu, T., Liang, E.-W., Gu, W.-M., Zhao, X.-H., Dai, Z.-G., & Lu, J.-F. 2010, arXiv:1003.4883
- Lu, R., & Liang, E. 2010, Science in China G: Physics and Astronomy, 53, 163
- Medvedev, M. V. 2006, ApJ, 637, 869
- Mallozzi, R. S., Preece, R. D., & Briggs, M. S. 2005, RMFIT, A Lightcurve and Spectral Analysis Tool, (Huntsville: Univ. Alabama)
- Nakar, E., & Piran, T. 2005, MNRAS, 360, L73
- Norris, J. P., Share, G. H., Messina, D. C., Dennis, B. R., Desai, U. D., Cline, T. L., Matz, S. M., & Chupp, E. L. 1986, ApJ, 301, 213
- Ohno, M., Ioka, K., Yamaoka, K., Tashiro, M., Fukazawa, Y., & Nakagawa, Y. E. 2009, PASJ, 61, 201
- Panaitescu, A., Meszaros, P., & Rees, M. J. 1998, ApJ, 503, 314
- Panaitescu, A., & Vestrand, W. T. 2008, MNRAS, 387, 497
- Peng, Z. Y., Ma, L., Zhao, X. H., Yin, Y., Fang, L. M., & Bao, Y. Y. 2009, ApJ, 698, 417
- Portegies Zwart, S. F., Lee, C.-H., & Lee, H. K. 1999, A&AS, 138, 503
- Preece, R. D., Briggs, M. S., Mallozzi, R. S., Pendleton, G. N., Paciesas, W. S., & Band, D. L. 1998, ApJ, 506, L23
- Qin, Y.-P. 2008, ApJ, 683, 900
- Qin, Y.-P. 2002, A&A, 396, 705
- Reynoso, M. M., Romero, G. E., & Sampayo, O. A. 2006, A&A, 454, 11
- Sakamoto, T., et al. 2006, ApJ, 636, L73
- Shahmoradi, A., & Nemiroff, R. J. 2009, arXiv:0904.1464
- Shen, R.-F., Song, L.-M., & Li, Z. 2005, MNRAS, 362, 59
- Toma, K., Ioka, K., Sakamoto, T., & Nakamura, T. 2007, ApJ, 659, 1420
- Wei, D. M., & Gao, W. H. 2003, MNRAS, 345, 743
- Yonetoku, D., Murakami, T., Nakamura, T., Yamazaki, R., Inoue, A. K., & Ioka, K. 2004, ApJ, 609, 935
- Zhang, B.-B., Zhang, B., Liang, E.-W., & Wang, X.-Y. 2009, ApJ, 690, L10
- Zhang, B., & Mészáros, P. 2002, ApJ, 581, 1236
- Zhang, B., & Mészáros, P. 2004, International Journal of Modern Physics A, 19, 2385

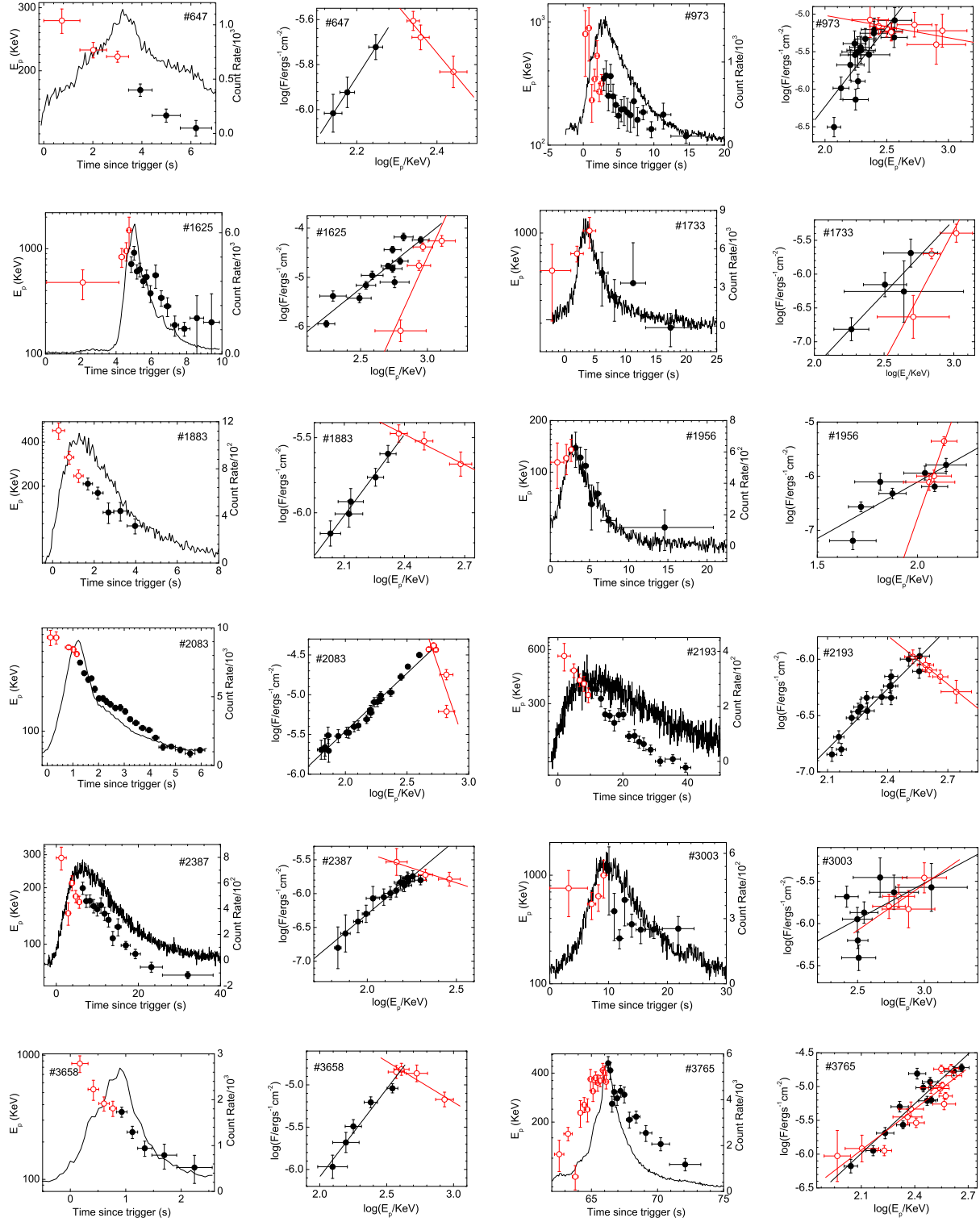


Fig. 1.— Lightcurves with E_p evolution (circles) (*left Panels*) and $F - E_p$ correlations (*right panels*) for the pulses in our sample. The open circles are for the rising phase and the solid circles are for decaying phase. Lines are the best fits to the $F - E_p$ correlation.

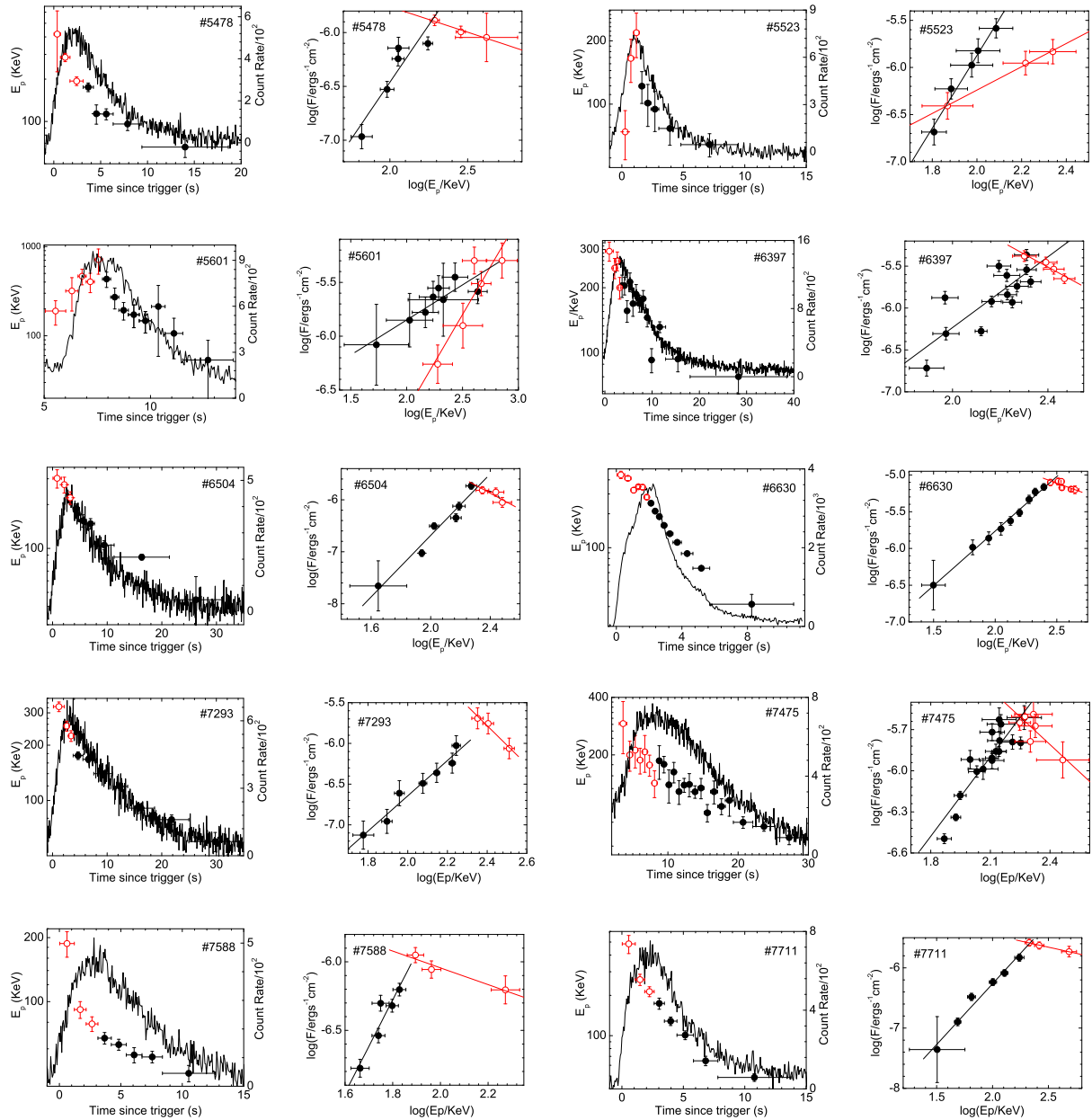


Fig. 1.— *Continued.*

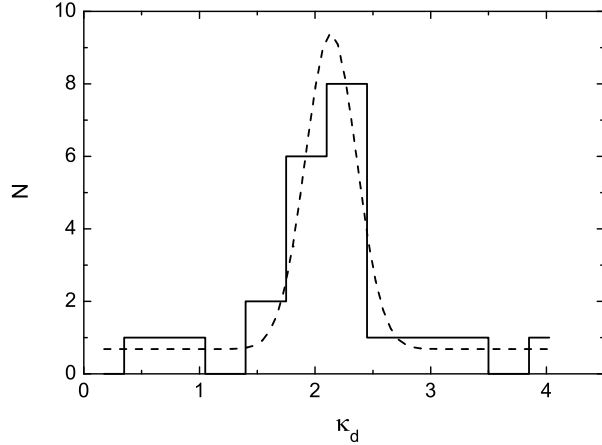


Fig. 1.— Distribution of κ_d (the *solid* step line) for the pulses in our sample. The *dashed* line is the Gaussian fit, which yields $\kappa_d = 2.14 \pm 0.44$ (1σ).

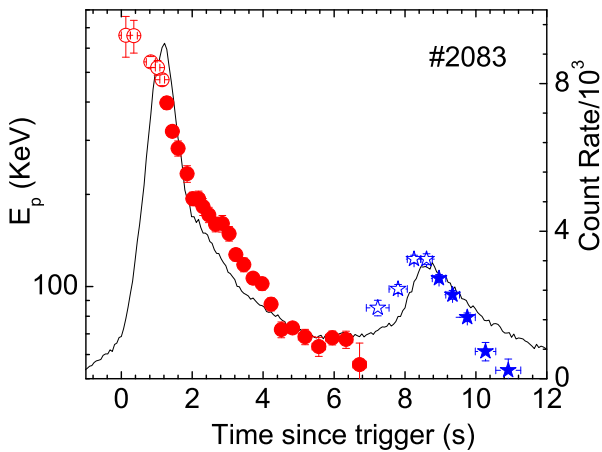


Fig. 2.— The lightcurves and spectral evolution (circles and stars) for two well-separated pulses in #2083.

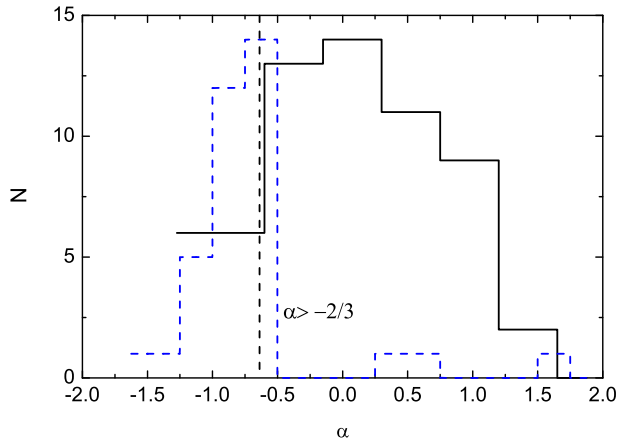


Fig. 3.— Distribution of the low energy photon indices (α) in the spectra whose E_p is anti-correlated with the observed fluxes (solid step line). The α distribution of the spectra whose E_p is correlated with the observed fluxes (dashed line) in the same pulses are also shown for comparison. The death line ($\alpha = -2/3$) of the synchrotron radiation is shown with a vertical dashed line.

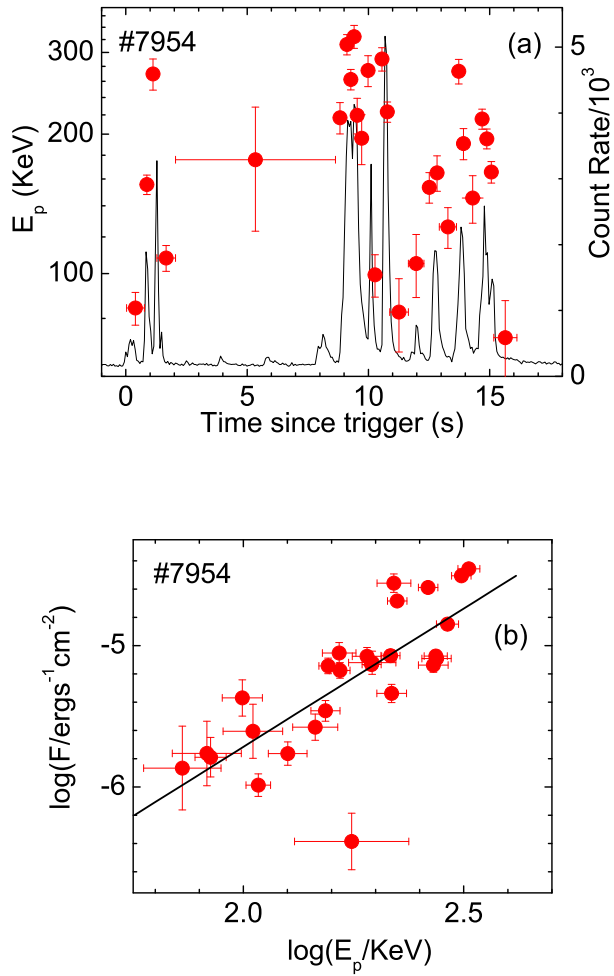


Fig. 4.— Example (#7954) of time-resolved spectra analysis for multi-pulses GRBs and the $F - E_p$ correlation within the GRB. The symbols and line style are the same as Fig. 1.

TABLE 1

THE POWER-LAW INDICES OF THE $F \propto E_p^{\kappa_r(\kappa_d)}$ RELATION FOR THE PULSES IN OUR SAMPLE. N AND r ARE THE NUMBER OF THE DATA POINTS AND THE CORRELATION COEFFICIENT, RESPECTIVELY.

Trigger#	κ_r	r	N	κ_d	r	N
647	-2.137±0.321	-0.988	3	2.775±0.049	0.999	3
973	-0.297±0.150	-0.662	7	2.118±0.422	0.791	17
1733	3.877±1.506	0.932	3	2.176±0.758	0.896	4
1883	-0.671±0.121	-0.983	3	1.796±0.141	0.99	5
1956	10.55±2.011	0.982	3	2.09±0.643	0.823	7
2083	-4.515±1.712	-0.835	5	1.461±0.060	0.983	21
2193	-1.432±0.068	-0.996	5	1.783±0.148	0.954	16
2387	-0.871±0.201	-0.974	3	2.205±0.137	0.973	16
3003	1.097±0.707	0.738	4	0.854±0.544	0.539	8
3658	-0.963±0.253	-0.937	4	2.076±0.272	0.975	5
3765	2.0248±0.249	0.919	14	2.449±0.299	0.932	12
5478	-0.473±0.092	-0.981	3	2.123±0.569	0.906	5
5523	1.237±0.062	0.998	3	3.857±0.339	0.988	5
5601	1.779±0.491	0.902	5	0.651±0.135	0.89	8
6397	-1.55±0.341	-0.954	4	2.110±0.465	0.807	13
6504	-1.547±1.01	-0.837	3	2.961±0.300	0.979	6
6630	-0.606±0.217	-0.812	6	1.483±0.051	0.995	9
7293	-2.401±0.422	-0.984	3	2.166±0.204	0.978	7
7475	-1.345±0.506	-0.799	6	1.927±0.26	0.885	17
7588	-0.612±0.161	-0.966	3	3.399±0.765	0.931	5
7711	-0.410±0.032	-0.997	3	2.015±0.16	0.987	6

TABLE 2

ONLINE MATERIAL: SPECTRAL FITS WITH THE BAND FUNCTION. THE FLUX IS IN THE $30 - 10^4$ keV BAND.

Trigger#	t_{start} (s)	t_{end} (s)	E_p (keV)	α	β	flux (10^{-6} erg/cm 2 s)
647	0	1.472	276.06 ± 21.61	0.53 ± 0.24	-2.65 ± 0.28	1.47 ± 0.24
647	1.472	2.56	228.64 ± 11.35	0.74 ± 0.2	-2.86 ± 0.23	2.09 ± 0.26
647	2.56	3.456	219.13 ± 7.88	0.75 ± 0.16	-3.4 ± 0.34	2.48 ± 0.24
647	3.456	4.416	176.7 ± 7.02	0.63 ± 0.19	-3.16 ± 0.26	1.9 ± 0.24
647	4.416	5.568	150.05 ± 6.32	0.44 ± 0.22	-3.33 ± 0.36	1.19 ± 0.19
647	5.568	6.848	138.34 ± 7.03	0.26 ± 0.27	-3.14 ± 0.32	0.96 ± 0.19
973	0	0.576	797.06 ± 435.63	-0.99 ± 0.15	-1.76 ± 0.29	3.93 ± 2.37
973	0.576	1.024	891.13 ± 410.27	-1.02 ± 0.11	-1.82 ± 0.31	6 ± 3.01
973	1.024	1.408	231.82 ± 78.66	-0.49 ± 0.35	-1.57 ± 0.06	8.39 ± 4.54
973	1.408	1.792	343.63 ± 68.95	-0.73 ± 0.15	-1.93 ± 0.13	5.75 ± 1.55
973	1.792	2.112	530.62 ± 172.22	-1.03 ± 0.12	-1.89 ± 0.19	7.21 ± 2.71
973	2.112	2.432	271.79 ± 45.74	-0.5 ± 0.19	-1.9 ± 0.1	6.92 ± 1.8
973	2.432	2.752	315.61 ± 57.94	-0.65 ± 0.16	-1.95 ± 0.13	6.42 ± 1.66
973	2.752	3.072	346.97 ± 69.75	-0.9 ± 0.13	-2.05 ± 0.17	5.93 ± 1.55
973	3.072	3.392	366.84 ± 116.22	-1.01 ± 0.15	-1.79 ± 0.1	8.25 ± 3.23
973	3.392	3.712	250.95 ± 60.93	-0.84 ± 0.2	-1.87 ± 0.1	6.22 ± 2.19
973	3.712	4.032	362.95 ± 89.4	-1.03 ± 0.13	-2.08 ± 0.22	4.89 ± 1.51
973	4.032	4.416	248.49 ± 63.74	-0.91 ± 0.2	-1.86 ± 0.09	5.56 ± 2.03
973	4.416	4.8	212.21 ± 41.97	-0.73 ± 0.22	-1.95 ± 0.1	4.67 ± 1.5
973	4.8	5.184	173.57 ± 37.11	-0.71 ± 0.3	-1.95 ± 0.09	4.05 ± 1.58
973	5.184	5.568	194.21 ± 39.52	-0.77 ± 0.25	-2.01 ± 0.11	3.6 ± 1.24
973	5.568	6.016	195.96 ± 51.96	-1.04 ± 0.24	-1.99 ± 0.11	3.3 ± 1.33
973	6.016	6.464	184.43 ± 54.69	-0.99 ± 0.29	-1.95 ± 0.11	3.14 ± 1.47
973	6.464	6.912	174.99 ± 48	-0.87 ± 0.33	-1.96 ± 0.11	2.86 ± 1.34
973	6.912	7.424	227.09 ± 87.91	-1.14 ± 0.25	-1.91 ± 0.12	2.87 ± 1.52
973	7.424	7.936	160.46 ± 41.02	-0.88 ± 0.35	-2.04 ± 0.13	2.1 ± 0.98
973	7.936	9.024	185.24 ± 24.39	-1.09 ± 0.16	-2.48 ± 0.3	1.28 ± 0.27
973	9.024	10.24	134.8 ± 20	-0.73 ± 0.32	-2.25 ± 0.14	1.03 ± 0.36
973	10.24	12.416	176.9 ± 41.82	-1.57 ± 0.15	-2.49 ± 0.65	0.73 ± 0.23
973	12.416	16.704	118.23 ± 14.67	-1.11 ± 0.29	-2.61 ± 0.38	0.31 ± 0.09
1625	0.064	4.16	630.13 ± 277.92	-0.99 ± 0.16	-2.02 ± 0.5	0.82 ± 0.41
1625	4.16	4.48	865.53 ± 173.67	-0.63 ± 0.08	-2.1 ± 0.17	17.32 ± 3.97
1625	4.48	4.672	926.02 ± 156.35	-0.52 ± 0.07	-2.11 ± 0.16	41.34 ± 7.75
1625	4.672	4.8	1281.55 ± 300.49	-0.63 ± 0.07	-2.27 ± 1.8	54.93 ± 13.7
1625	4.8	4.928	663.63 ± 108.87	-0.42 ± 0.1	-1.75 ± 0.11	65.92 ± 11.73
1625	4.928	5.12	892.01 ± 128.88	-0.67 ± 0.06	-1.98 ± 0.19	57.54 ± 8.97
1625	5.12	5.248	548.89 ± 79.89	-0.58 ± 0.09	-2.02 ± 0.16	36.32 ± 5.68
1625	5.248	5.44	625.82 ± 85.39	-0.83 ± 0.07	-2.37 ± 0.33	21.29 ± 3.12
1625	5.44	5.632	508.13 ± 60.76	-0.75 ± 0.07	-2.44 ± 0.3	16.95 ± 2.19
1625	5.632	5.824	548.99 ± 89.78	-0.92 ± 0.08	-2.32 ± 0.32	14.96 ± 2.58
1625	5.824	6.08	386.59 ± 72.37	-1.02 ± 0.1	-2.08 ± 0.16	10.95 ± 2.15

TABLE 2—Continued

Trigger#	t_{start} (s)	t_{end} (s)	E_p (keV)	α	β	flux (10^{-6} erg/cm 2 s)
1625	6.08	6.4	568.82 ± 142.06	-1.21 ± 0.08	-2.25 ± 0.4	7.95 ± 2.06
1625	6.4	6.72	347.37 ± 58.06	-0.86 ± 0.12	-2.14 ± 0.18	6.87 ± 1.21
1625	6.72	7.104	310.33 ± 62.73	-1.13 ± 0.12	-2.33 ± 0.33	3.76 ± 0.79
1625	7.104	7.552	196.74 ± 44.88	-0.8 ± 0.24	-1.93 ± 0.1	4.15 ± 0.99
1625	7.552	8.96	175.43 ± 25.46	-0.92 ± 0.19	-2.33 ± 0.22	1.13 ± 0.17
1733	-5.12	1.024	511.7 ± 304	-1.2 ± 0.18	-7.14 ± 6	0.23 ± 0.17
1733	1.024	3.072	693.1 ± 96.9	-1.53 ± 0.1	-1.9 ± 0.17	2 ± 0.35
1733	3.072	5.12	1042 ± 280	-1.03 ± 0.05	-1.98 ± 0.39	4.02 ± 1.23
1733	5.12	7.168	490.8 ± 219	-1.23 ± 0.11	-1.77 ± 0.14	2.05 ± 0.98
1733	7.168	9.216	320.8 ± 114	-1.14 ± 0.17	-2.13 ± 0.44	0.7 ± 0.29
1733	13.312	21.504	184.2 ± 53.1	-0.78 ± 0.37	-2.28 ± 0.52	0.15 ± 0.06
1883	0	0.576	478.5 ± 60.9	-0.11 ± 0.17	-3.13 ± 1.15	2.11 ± 0.39
1883	0.576	1.024	314.7 ± 31.6	-0.15 ± 0.16	-2.63 ± 0.34	3 ± 0.41
1883	1.024	1.472	235.2 ± 23	-0.27 ± 0.18	-2.27 ± 0.23	3.37 ± 0.45
1883	1.472	1.92	207.8 ± 19.3	-0.36 ± 0.18	-2.58 ± 0.26	2.47 ± 0.32
1883	1.92	2.432	180.1 ± 16.7	-0.88 ± 0.15	-3.02 ± 0.65	1.72 ± 0.23
1883	2.432	2.944	132.7 ± 21.1	-0.33 ± 0.32	-2.57 ± 0.15	0.98 ± 0.2
1883	2.944	3.584	135.5 ± 19.6	-1.23 ± 0.22	-2.63 ± 0.45	1.19 ± 0.24
1883	3.584	4.352	107.3 ± 12.6	-1.27 ± 0.26	-3.01 ± 0.97	0.73 ± 0.14
1956	0.064	1.728	114.2 ± 33.7	-0.65 ± 0.56	-1.97 ± 0.11	0.78 ± 0.27
1956	1.728	2.368	120.8 ± 24.2	-0.6 ± 0.33	-2.2 ± 0.17	1 ± 0.25
1956	2.368	2.944	135.6 ± 20.1	0.37 ± 0.96	-1.91 ± 0.07	4.43 ± 0.85
1956	2.944	3.52	138.8 ± 32.2	-0.87 ± 0.33	-2.08 ± 0.13	1.61 ± 0.45
1956	3.52	4.16	121.7 ± 18.2	-0.59 ± 0.25	-2.64 ± 0.39	0.64 ± 0.14
1956	4.16	4.864	108.9 ± 26.5	-0.64 ± 0.52	-2.08 ± 0.12	1.14 ± 0.34
1956	4.864	5.632	65.13 ± 19.1	0.37 ± 1.92	-2.08 ± 0.09	0.78 ± 0.28
1956	5.632	6.464	74.97 ± 11.7	0.62 ± 1.2	-2.38 ± 0.15	0.48 ± 0.11
2083	0	0.256	660.98 ± 100.06	-0.74 ± 0.08	-5.14 ± 6.72	6.15 ± 1.1
2083	0.256	0.448	658.86 ± 80.9	-0.58 ± 0.07	-2.45 ± 0.37	17.84 ± 2.63
2083	0.704	0.96	541.2 ± 21.95	-0.13 ± 0.05	-3.27 ± 0.37	36.71 ± 2.01
2083	0.96	1.088	518.05 ± 28.76	-0.14 ± 0.06	-3.15 ± 0.41	41.49 ± 3.14
2083	1.088	1.216	473.24 ± 20.47	-0.1 ± 0.06	-4.18 ± 1.13	37.12 ± 2.29
2083	1.216	1.344	397.75 ± 18.48	-0.06 ± 0.07	-3.4 ± 0.43	31.52 ± 2.22
2083	1.344	1.536	321.28 ± 12.52	-0.13 ± 0.06	-3.29 ± 0.31	22.55 ± 1.45
2083	1.536	1.664	282.47 ± 16.13	-0.36 ± 0.09	-3.07 ± 0.33	16.72 ± 1.58
2083	1.792	1.92	233.34 ± 14.64	-0.49 ± 0.11	-3.07 ± 0.38	10.68 ± 1.2
2083	1.92	2.112	193.38 ± 9.8	-0.23 ± 0.12	-2.74 ± 0.17	9.77 ± 1.07
2083	2.112	2.24	193.46 ± 11.33	-0.19 ± 0.14	-2.88 ± 0.25	8.75 ± 1.13
2083	2.24	2.368	182.1 ± 11.48	-0.36 ± 0.15	-2.85 ± 0.25	8.14 ± 1.13
2083	2.368	2.56	171.41 ± 9.84	-0.32 ± 0.14	-2.64 ± 0.15	8.05 ± 1.07
2083	2.56	2.752	159.63 ± 8.85	-0.5 ± 0.14	-2.85 ± 0.22	6.44 ± 0.84

TABLE 2—*Continued*

Trigger#	t_{start} (s)	t_{end} (s)	E_p (keV)	α	β	flux (10^{-6} erg/cm 2 s)
2083	2.752	2.944	160.6 ± 10.07	-0.8 ± 0.13	-2.93 ± 0.31	5.92 ± 0.78
2083	2.944	3.136	148.76 ± 8.08	-0.91 ± 0.12	-3.41 ± 0.69	4.9 ± 0.58
2083	3.136	3.328	127.1 ± 5.93	-0.7 ± 0.15	-3.36 ± 0.49	4.1 ± 0.55
2083	3.328	3.584	117.85 ± 6.14	-0.89 ± 0.16	-2.97 ± 0.28	3.95 ± 0.57
2083	3.584	3.84	106.5 ± 4.62	-0.62 ± 0.19	-3.1 ± 0.27	3.33 ± 0.53
2083	3.84	4.096	102.21 ± 4.95	-1.06 ± 0.17	-3.18 ± 0.43	3.34 ± 0.49
2083	4.096	4.352	87.5 ± 4.3	-1.03 ± 0.22	-3.04 ± 0.3	3.01 ± 0.56
2083	4.352	4.672	72.33 ± 4.27	-1.18 ± 0.27	-2.78 ± 0.17	3.08 ± 0.74
2083	4.672	4.992	73.2 ± 2.92	-0.27 ± 0.41	-3.03 ± 0.17	1.97 ± 0.66
2083	4.992	5.376	68.51 ± 3.95	-1.06 ± 0.28	-2.99 ± 0.22	2.18 ± 0.55
2083	5.376	5.76	63.7 ± 4.52	-1.1 ± 0.3	-3.1 ± 0.26	2.03 ± 0.56
2083	5.76	6.144	68.02 ± 3.57	-0.92 ± 0.35	-2.9 ± 0.18	2.08 ± 0.62
2193	0	3.84	552.6 ± 96.4	0.18 ± 0.19	-3.75 ± 0.46	0.51 ± 0.12
2193	3.84	5.952	459.6 ± 40	0.1 ± 0.24	-3.12 ± 0.74	0.7 ± 0.09
2193	5.952	7.36	405.9 ± 32.7	0.87 ± 0.24	-4.08 ± 2.31	0.8 ± 0.11
2193	7.36	8.704	387.8 ± 36.5	0.67 ± 0.24	-3.16 ± 0.85	0.89 ± 0.13
2193	8.704	9.984	335.6 ± 31.4	1.06 ± 0.31	-2.59 ± 0.36	1.05 ± 0.15
2193	9.984	11.264	362.6 ± 41.2	0.54 ± 0.26	-2.51 ± 0.39	1.07 ± 0.17
2193	11.264	12.608	360.8 ± 27.3	0.5 ± 0.21	-3.19 ± 0.3	0.78 ± 0.11
2193	12.608	13.888	320.2 ± 31.1	0.76 ± 0.28	-2.56 ± 0.36	1 ± 0.14
2193	13.888	15.232	261.7 ± 19.5	1.26 ± 0.33	-2.88 ± 0.45	0.7 ± 0.09
2193	15.232	16.64	257.3 ± 18	1.31 ± 0.33	-3.2 ± 0.66	0.58 ± 0.08
2193	16.64	18.048	234.6 ± 22.8	1.56 ± 0.42	-3.17 ± 0.21	0.46 ± 0.07
2193	18.048	19.456	259.9 ± 21.4	0.76 ± 0.28	-3.04 ± 0.65	0.58 ± 0.08
2193	19.456	20.864	261.5 ± 16.4	0.79 ± 0.25	-6.04 ± 3.5	0.45 ± 0.06
2193	20.864	22.912	197.5 ± 12.9	1.59 ± 0.4	-2.81 ± 0.34	0.45 ± 0.06
2193	22.912	24.32	198.8 ± 15.9	0.97 ± 0.38	-3.28 ± 0.86	0.35 ± 0.06
2193	24.32	25.728	184.1 ± 14.4	1.05 ± 0.4	-3.05 ± 0.58	0.38 ± 0.06
2193	25.728	27.136	178.9 ± 14.6	0.97 ± 0.41	-3.07 ± 0.62	0.34 ± 0.06
2193	27.136	30.016	166.2 ± 10.3	1.62 ± 0.42	-3.06 ± 0.27	0.3 ± 0.04
2193	33.024	37.76	147.6 ± 8.34	1.56 ± 0.38	-3.13 ± 0.43	0.16 ± 0.02
2193	37.76	40.96	132.4 ± 7.57	1.32 ± 0.47	-3.86 ± 1.1	0.14 ± 0.02
2387	0	2.432	288.77 ± 40.35	0 ± 0.22	-1.9 ± 0.13	1.64 ± 0.39
2387	2.432	3.392	146.2 ± 19.99	0.78 ± 0.53	-1.78 ± 0.06	2.94 ± 1.34
2387	3.392	4.288	211.88 ± 19.35	-0.06 ± 0.2	-2.32 ± 0.18	1.9 ± 0.36
2387	4.288	5.184	179.97 ± 13.48	0.16 ± 0.21	-2.39 ± 0.15	1.81 ± 0.34
2387	5.184	6.016	167.83 ± 12.41	0.2 ± 0.23	-2.43 ± 0.16	1.71 ± 0.34
2387	6.016	6.848	199.05 ± 14.84	-0.2 ± 0.17	-2.69 ± 0.29	1.58 ± 0.25
2387	6.848	7.744	169.8 ± 12.81	-0.13 ± 0.2	-2.48 ± 0.18	1.66 ± 0.3
2387	7.744	8.64	170.23 ± 12.91	-0.13 ± 0.2	-2.52 ± 0.2	1.53 ± 0.28
2387	8.64	9.536	159.84 ± 13.21	-0.2 ± 0.22	-2.48 ± 0.19	1.44 ± 0.3

TABLE 2—*Continued*

Trigger#	t_{start} (s)	t_{end} (s)	E_p (keV)	α	β	flux (10^{-6} erg/cm 2 s)
2387	9.536	10.432	153.53 ± 12.32	0.04 ± 0.25	-2.42 ± 0.16	1.47 ± 0.33
2387	10.432	11.328	161.48 ± 15.23	-0.41 ± 0.22	-2.49 ± 0.22	1.32 ± 0.29
2387	11.328	12.224	145.46 ± 11.8	-0.22 ± 0.25	-2.61 ± 0.24	1.11 ± 0.25
2387	12.224	13.248	134.81 ± 11.2	-0.47 ± 0.24	-2.63 ± 0.25	1.01 ± 0.23
2387	13.248	14.272	107.57 ± 9.32	0.4 ± 0.49	-2.47 ± 0.15	0.85 ± 0.35
2387	14.272	15.808	123.71 ± 12.88	-0.62 ± 0.28	-2.41 ± 0.17	0.89 ± 0.25
2387	15.808	18.048	98.49 ± 4.85	0.47 ± 0.37	-2.87 ± 0.18	0.5 ± 0.15
2387	18.048	20.48	88.73 ± 5.13	0.27 ± 0.47	-2.86 ± 0.21	0.39 ± 0.15
2387	20.48	25.856	75.48 ± 4.58	0.96 ± 0.76	-2.73 ± 0.14	0.26 ± 0.16
2387	25.856	38.208	68.4 ± 2.88	1.36 ± 0.89	-2.51 ± 0.35	0.16 ± 0.11
3003	0	6.4	759.9 ± 345.34	-0.89 ± 0.13	-1.57 ± 0.13	1.48 ± 0.75
3003	6.4	7.808	542.53 ± 152.1	-0.85 ± 0.12	-2.73 ± 0.13	1.6 ± 0.53
3003	7.808	8.704	640.64 ± 175.73	-0.92 ± 0.1	-2.98 ± 0.28	2.1 ± 0.66
3003	8.704	9.6	997.36 ± 379.48	-1.11 ± 0.08	-2.1 ± 0.65	3.48 ± 1.42
3003	9.6	10.496	1126.81 ± 695.77	-1.28 ± 0.08	-2.61 ± 5.2	2.68 ± 1.74
3003	10.496	11.392	465.62 ± 215.46	-1.13 ± 0.14	-1.71 ± 0.11	3.51 ± 1.87
3003	11.392	12.288	261.84 ± 52.21	-0.83 ± 0.17	-2 ± 0.15	2.08 ± 0.59
3003	12.288	13.184	591.4 ± 250.03	-1.25 ± 0.1	-2.02 ± 0.36	2.34 ± 1.1
3003	13.184	14.656	353.46 ± 84.7	-1.2 ± 0.11	-2.25 ± 0.38	1.35 ± 0.39
3003	14.656	16.256	314.7 ± 80.18	-1.14 ± 0.13	-2.17 ± 0.31	1.13 ± 0.36
3003	16.256	19.136	317.1 ± 55.69	-1.22 ± 0.09	-3.25 ± 3.04	0.63 ± 0.14
3003	19.136	24.512	321.97 ± 94.62	-1.43 ± 0.11	-2.96 ± 3.3	0.39 ± 0.14
3658	0.026	0.32	856.5 ± 131	-0.3 ± 0.11	-3.25 ± 2.63	6.72 ± 1.34
3658	0.32	0.512	531.2 ± 97.8	-0.32 ± 0.14	-1.88 ± 0.17	13.68 ± 3.1
3658	0.512	0.704	408.1 ± 53.1	-0.02 ± 0.15	-1.9 ± 0.12	15.28 ± 2.49
3658	0.704	0.832	373.7 ± 52.4	-0.15 ± 0.16	-2.03 ± 0.16	14.2 ± 2.5
3658	0.832	1.024	349.3 ± 32.3	-0.25 ± 0.11	-2.49 ± 0.25	9.1 ± 1.13
3658	1.024	1.216	240.5 ± 27.3	-0.25 ± 0.17	-2.22 ± 0.17	6.22 ± 0.92
3658	1.216	1.472	178.1 ± 24.9	-0.48 ± 0.23	-2.22 ± 0.18	3.23 ± 0.59
3658	1.472	1.92	156.7 ± 35.6	-0.82 ± 0.29	-2.06 ± 0.14	2.08 ± 0.57
3658	1.92	2.56	124.6 ± 31.8	-0.73 ± 0.46	-2.11 ± 0.16	1.07 ± 0.34
3765	62.208	62.912	126.96 ± 27.61	-0.95 ± 0.36	-2.44 ± 0.13	1.21 ± 0.55
3765	62.912	63.552	169.45 ± 15.98	-1.02 ± 0.15	-3.61 ± 2.32	1.13 ± 0.2
3765	63.552	64	92.31 ± 15.69	0.68 ± 0.93	-3.43 ± 0.06	0.94 ± 0.82
3765	64	64.32	228.57 ± 42.74	-1.06 ± 0.16	-2.26 ± 0.23	3.55 ± 0.96
3765	64.32	64.576	255.67 ± 27.25	-0.93 ± 0.12	-3.8 ± 2.98	2.91 ± 0.47
3765	64.576	64.832	239.14 ± 38.74	-0.92 ± 0.15	-2.27 ± 0.21	4.64 ± 1.12
3765	64.832	65.024	367.07 ± 54.23	-0.92 ± 0.11	-2.83 ± 0.76	5.51 ± 1.06
3765	65.024	65.216	309.53 ± 42.03	-0.73 ± 0.12	-2.21 ± 0.17	9.58 ± 1.84
3765	65.216	65.408	374.47 ± 32.26	-0.84 ± 0.07	-4.43 ± 5.87	7.25 ± 0.84
3765	65.408	65.536	349.29 ± 40.22	-0.71 ± 0.11	-2.81 ± 0.51	9.35 ± 1.49

TABLE 2—*Continued*

Trigger#	t_{start} (s)	t_{end} (s)	E_p (keV)	α	β	flux (10^{-6} erg/cm 2 s)
3765	65.536	65.792	358.48 ± 28.66	-0.71 ± 0.07	-2.78 ± 0.33	10.39 ± 1.14
3765	65.792	65.92	416.84 ± 42.29	-0.69 ± 0.08	-2.87 ± 0.52	14.45 ± 1.94
3765	65.92	66.048	402.24 ± 39.42	-0.55 ± 0.09	-2.54 ± 0.27	18.63 ± 2.48
3765	66.048	66.176	353.8 ± 34.24	-0.56 ± 0.09	-2.46 ± 0.22	18.12 ± 2.48
3765	66.176	66.368	460.24 ± 44.61	-0.74 ± 0.07	-2.52 ± 0.27	19.03 ± 2.34
3765	66.368	66.496	415.71 ± 49.56	-0.75 ± 0.09	-2.51 ± 0.31	16.85 ± 2.61
3765	66.496	66.624	259.13 ± 28.85	-0.4 ± 0.15	-2.14 ± 0.12	15.52 ± 2.84
3765	66.624	66.816	306.45 ± 31.06	-0.69 ± 0.1	-2.37 ± 0.18	11.76 ± 1.72
3765	66.816	67.072	280.38 ± 26.84	-0.76 ± 0.09	-2.37 ± 0.16	9.6 ± 1.35
3765	67.072	67.328	310.7 ± 25.73	-0.89 ± 0.08	-3.42 ± 1.11	6.33 ± 0.73
3765	67.328	67.648	294.92 ± 32.75	-0.97 ± 0.09	-2.55 ± 0.29	6.15 ± 0.94
3765	67.648	68.096	206.78 ± 23.17	-0.89 ± 0.12	-2.24 ± 0.12	5.04 ± 0.9
3765	68.096	68.672	215.82 ± 18.2	-0.97 ± 0.1	-2.9 ± 0.48	2.71 ± 0.36
3765	68.672	69.568	171.33 ± 19.19	-1.05 ± 0.14	-2.4 ± 0.19	2.05 ± 0.39
3765	69.568	70.912	146.77 ± 13.54	-1.14 ± 0.14	-2.72 ± 0.38	1.13 ± 0.19
3765	70.912	73.28	109.87 ± 9.59	-1 ± 0.23	-2.6 ± 0.23	0.67 ± 0.15
5478	0.029	0.704	418.7 ± 193	-0.29 ± 0.38	-3.51 ± 0.15	0.9 ± 0.47
5478	0.704	1.728	285.9 ± 19.4	0.05 ± 0.15	-10.94 ± 80	1.02 ± 0.12
5478	1.728	3.136	193.9 ± 13.6	0.51 ± 0.22	-2.48 ± 0.21	1.3 ± 0.15
5478	3.136	4.224	175.5 ± 12.4	0.25 ± 0.24	-3.01 ± 0.72	0.79 ± 0.11
5478	4.224	4.864	113.4 ± 17.7	0.86 ± 0.85	-2.4 ± 0.18	0.72 ± 0.17
5478	4.864	6.336	112.9 ± 10.1	1.5 ± 0.69	-2.45 ± 0.18	0.57 ± 0.09
5478	6.336	9.408	95.91 ± 9.67	1.62 ± 0.94	-2.47 ± 0.19	0.3 ± 0.05
5478	9.408	18.624	65.75 ± 10.3	0.04 ± 1.36	-2.6 ± 0.28	0.11 ± 0.03
5523	0.033	0.512	73.84 ± 19.4	1.61 ± 2.36	-4.92 ± 0.09	0.39 ± 0.13
5523	0.512	0.96	165.1 ± 38.3	-0.55 ± 0.36	-3.54 ± 0.17	1.11 ± 0.32
5523	0.96	1.408	218.6 ± 52.2	-0.95 ± 0.22	-3.25 ± 0.35	1.47 ± 0.44
5523	1.408	1.856	121.8 ± 21	0.09 ± 0.79	-2.08 ± 0.13	2.6 ± 0.61
5523	1.856	2.368	101.2 ± 22.8	-0.02 ± 0.83	-2.1 ± 0.14	1.5 ± 0.44
5523	2.368	3.008	94.75 ± 20.6	-0.09 ± 0.86	-2.19 ± 0.17	1.06 ± 0.31
5523	3.008	4.8	76.69 ± 12.9	-0.11 ± 0.98	-2.21 ± 0.2	0.59 ± 0.15
5523	4.8	9.472	64.26 ± 8.14	0.15 ± 1.58	-2.12 ± 1.68	0.21 ± 0.06
5601	5.056	6.016	189.6 ± 57.8	-1.26 ± 0.21	-3.19 ± 0.4	0.55 ± 0.22
5601	6.016	6.592	318.4 ± 129	-0.95 ± 0.17	-2.4 ± 0.94	1.25 ± 0.6
5601	6.592	6.976	465.2 ± 92.5	-0.66 ± 0.16	-2.67 ± 0.83	3.08 ± 0.79
5601	6.976	7.36	403.1 ± 99	-0.61 ± 0.19	-1.98 ± 0.2	5.04 ± 1.44
5601	7.36	7.744	713.8 ± 224	-0.91 ± 0.13	-2.23 ± 0.61	5.04 ± 1.88
5601	7.744	8.128	432.3 ± 84.6	-0.99 ± 0.12	-6.74 ± 7	2.6 ± 0.68
5601	8.128	8.512	271.1 ± 71.3	-0.76 ± 0.24	-2.05 ± 0.18	3.54 ± 1.07
5601	8.512	8.96	193.1 ± 42.8	-0.65 ± 0.31	-2.07 ± 0.16	2.8 ± 0.74
5601	8.96	9.472	172.5 ± 49.3	-0.98 ± 0.32	-2.08 ± 0.16	2.32 ± 0.77

TABLE 2—Continued

Trigger#	t_{start} (s)	t_{end} (s)	E_p (keV)	α	β	flux (10^{-6} erg/cm 2 s)
5601	9.472	10.048	147.1 ± 39.8	-1.02 ± 0.37	-2.18 ± 0.2	2.32 ± 0.77
5601	10.048	10.688	212.8 ± 154	-1.42 ± 0.41	-1.87 ± 0.14	1.67 ± 0.54
5601	10.688	11.52	106.4 ± 51	-1.45 ± 1.05	-1.94 ± 0.11	1.67 ± 0.54
5601	11.52	13.888	53.59 ± 35.5	-1.48 ± 3.28	-2.03 ± 0.07	2.18 ± 1.7
6397	0.092	1.792	294.6 ± 29.9	-0.4 ± 0.11	-2.17 ± 0.18	2.24 ± 0.29
6397	1.792	2.368	246.4 ± 26.3	-0.28 ± 0.15	-2.17 ± 0.17	3.52 ± 0.5
6397	2.368	2.88	265.8 ± 26.4	-0.53 ± 0.12	-2.59 ± 0.38	2.92 ± 0.4
6397	2.88	3.392	200.1 ± 22.8	-0.24 ± 0.19	-2.03 ± 0.11	4.17 ± 0.62
6397	3.392	3.904	204.5 ± 24	-0.26 ± 0.19	-2.01 ± 0.11	4.3 ± 0.65
6397	3.904	4.416	204.4 ± 19.2	-0.28 ± 0.16	-2.34 ± 0.2	2.87 ± 0.38
6397	4.416	4.992	156.5 ± 17.9	-0.1 ± 0.25	-2.04 ± 0.1	3.18 ± 0.48
6397	4.992	5.632	212.7 ± 21.2	-0.56 ± 0.14	-2.54 ± 0.33	2.07 ± 0.3
6397	5.632	6.272	168.9 ± 21.2	-0.49 ± 0.2	-2.15 ± 0.14	2.45 ± 0.41
6397	6.272	6.976	186.4 ± 20.4	-0.74 ± 0.15	-2.48 ± 0.3	1.82 ± 0.28
6397	6.976	7.744	169.7 ± 15.3	-0.54 ± 0.16	-2.64 ± 0.35	1.45 ± 0.2
6397	7.744	8.512	178 ± 16.2	-0.72 ± 0.14	-3.1 ± 0.94	1.17 ± 0.18
6397	8.512	9.408	145.7 ± 13.7	-0.47 ± 0.2	-2.52 ± 0.26	1.2 ± 0.18
6397	9.408	10.368	92.93 ± 11.8	0.48 ± 0.62	-2.1 ± 0.09	1.33 ± 0.23
6397	10.368	12.864	131.8 ± 7.56	-0.64 ± 0.15	-3.52 ± 1.21	0.53 ± 0.06
6397	12.864	18.048	93.83 ± 11.9	-0.52 ± 0.37	-2.21 ± 0.1	0.49 ± 0.08
6397	18.048	38.464	77.83 ± 13	-0.24 ± 0.71	-2.17 ± 0.1	0.19 ± 0.04
6504	0.09	1.6	302.6 ± 43.5	0.66 ± 0.39	-2.5 ± 0.59	0.89 ± 0.19
6504	1.6	2.688	273.7 ± 34	0.48 ± 0.29	-2.4 ± 0.33	1.4 ± 0.25
6504	2.688	3.776	222.4 ± 21.8	1.53 ± 0.33	-2.08 ± 0.34	1.53 ± 0.25
6504	3.776	4.928	187.1 ± 15.4	1.81 ± 0.78	-2.65 ± 0.17	1.85 ± 0.27
6504	4.928	6.208	155 ± 14.9	1.05 ± 0.5	-2.48 ± 0.28	0.75 ± 0.13
6504	6.208	7.68	147.8 ± 12.1	1.14 ± 0.5	-2.96 ± 0.53	0.45 ± 0.08
6504	11.264	21.376	87.2 ± 3.97	0.43 ± 0.47	-5.94 ± 13.8	0.09 ± 0.01
6504	21.376	31.104	44.51 ± 19.6	1.29 ± 14.6	-2.93 ± 1	0.02 ± 0.02
6630	0.042	0.512	443.1 ± 33.28	0.85 ± 0.19	-2.62 ± 0.27	6.28 ± 0.75
6630	0.512	0.896	412.24 ± 18.16	0.81 ± 0.13	-4.3 ± 1.28	6.4 ± 0.48
6630	0.896	1.216	323.82 ± 17.42	1.06 ± 0.18	-2.71 ± 0.2	8.14 ± 0.88
6630	1.216	1.472	347.15 ± 13.32	0.78 ± 0.13	-5.96 ± 6.63	6.7 ± 0.49
6630	1.472	1.728	344.24 ± 17.54	0.43 ± 0.12	-3.43 ± 0.52	8.14 ± 0.73
6630	1.728	1.984	280.55 ± 13.14	0.62 ± 0.14	-2.99 ± 0.33	7.9 ± 0.77
6630	1.984	2.24	248.16 ± 11.44	0.6 ± 0.15	-3.1 ± 0.29	6.84 ± 0.72
6630	2.24	2.496	210.98 ± 9.14	0.54 ± 0.16	-3.16 ± 0.29	5.88 ± 0.66
6630	2.496	2.752	188.49 ± 9.56	0.11 ± 0.16	-3.13 ± 0.33	4.65 ± 0.6
6630	2.752	3.072	157.58 ± 5.41	0.36 ± 0.17	-4 ± 0.73	3.06 ± 0.36
6630	3.072	3.456	133.01 ± 4.28	0.34 ± 0.19	-3.93 ± 0.6	2.37 ± 0.32
6630	3.456	3.968	111.32 ± 3.84	0.62 ± 0.26	-3.35 ± 0.25	1.85 ± 0.36

TABLE 2—Continued

Trigger#	t_{start} (s)	t_{end} (s)	E_p (keV)	α	β	flux (10^{-6} erg/cm 2 s)
6630	3.968	4.672	88.63 ± 2.66	-0.05 ± 0.26	-3.58 ± 0.34	1.38 ± 0.27
6630	4.672	5.696	65.6 ± 2.28	-0.38 ± 0.28	-4.2 ± 0.51	1.04 ± 0.24
6630	5.696	10.816	31.52 ± 6.97	-0.14 ± 1.13	-5 ± 0.19	0.32 ± 0.39
7293	0.162	2.176	324.3 ± 19.4	0.4 ± 0.15	-4.38 ± 2.98	0.87 ± 0.05
7293	2.176	3.008	254.2 ± 15.8	1.02 ± 0.29	-2.75 ± 0.34	1.75 ± 0.11
7293	3.008	3.776	224.7 ± 15	0.89 ± 0.26	-2.22 ± 0.42	2.03 ± 0.14
7293	3.776	5.568	175.6 ± 8.51	1.05 ± 0.24	-2.72 ± 0.2	0.94 ± 0.05
7293	5.568	7.552	167.5 ± 6.31	0.77 ± 0.19	-3.94 ± 0.94	0.57 ± 0.03
7293	7.552	11.008	139.9 ± 4.65	0.99 ± 0.21	-3.45 ± 0.39	0.44 ± 0.02
7293	11.008	13.76	119.2 ± 5.43	1.1 ± 0.35	-3.24 ± 0.36	0.32 ± 0.02
7293	13.76	18.688	90.75 ± 5.14	1.76 ± 0.64	-2.74 ± 0.16	0.24 ± 0.01
7475	3.072	4.16	291.5 ± 88.8	-1.42 ± 0.11	-2.61 ± 1.41	1.2 ± 0.37
7475	4.16	4.992	200 ± 35.8	-1.13 ± 0.14	-2.31 ± 0.31	1.64 ± 0.29
7475	4.992	5.696	212 ± 41.3	-1.19 ± 0.13	-2.24 ± 0.27	2.12 ± 0.41
7475	5.696	6.4	187.8 ± 28.8	-1.14 ± 0.13	-2.13 ± 0.26	2.49 ± 0.38
7475	6.4	7.04	207.5 ± 45.3	-1.34 ± 0.12	-2.15 ± 0.28	2.58 ± 0.56
7475	7.04	7.744	177 ± 22.3	-1.24 ± 0.11	-2.27 ± 0.56	2.24 ± 0.28
7475	7.744	8.448	142.3 ± 22.8	-1.22 ± 0.16	-2.24 ± 0.17	2.19 ± 0.35
7475	8.448	9.088	186.3 ± 37.2	-1.27 ± 0.14	-2.2 ± 0.21	2.44 ± 0.49
7475	9.088	9.792	178.7 ± 17.7	-1.33 ± 0.09	-6.48 ± 72	1.6 ± 0.16
7475	9.792	10.496	139.5 ± 27.6	-1.25 ± 0.19	-2.14 ± 0.13	2.36 ± 0.47
7475	10.496	11.2	162.7 ± 19.9	-1.28 ± 0.12	-2.78 ± 0.72	1.62 ± 0.2
7475	11.2	11.968	128.5 ± 18.3	-1.22 ± 0.17	-2.3 ± 0.17	1.91 ± 0.27
7475	11.968	12.672	139 ± 11.6	-1.24 ± 0.12	-3.51 ± 2.37	1.38 ± 0.12
7475	12.672	13.44	140.1 ± 19.5	-1.12 ± 0.17	-2.35 ± 0.22	1.66 ± 0.23
7475	13.44	14.272	128.2 ± 9.6	-1.37 ± 0.11	-8.56 ± 5	1.24 ± 0.09
7475	14.272	15.168	134.2 ± 16.3	-1.61 ± 0.1	-16.72 ± 8	1.38 ± 0.17
7475	15.168	16.064	99.57 ± 10.4	-0.8 ± 0.28	-2.4 ± 0.15	1.21 ± 0.18
7475	16.064	17.088	128.4 ± 17.6	-1.64 ± 0.11	-11.77 ± 8	1.19 ± 0.16
7475	17.088	18.176	107.6 ± 10.3	-1.56 ± 0.12	-23 ± 8	0.99 ± 0.09
7475	18.176	19.328	115.7 ± 20.1	-1.66 ± 0.14	-2.7 ± 1.16	1.03 ± 0.18
7475	19.328	22.08	88.74 ± 6.17	-1.36 ± 0.15	-2.78 ± 0.4	0.66 ± 0.05
7475	22.08	25.28	84.39 ± 4.69	-1.32 ± 0.13	-9.93 ± 8	0.46 ± 0.03
7475	25.28	29.248	73.83 ± 6.05	-1.39 ± 0.17	-19.39 ± 8	0.32 ± 0.03
7588	0.029	1.216	187.4 ± 25.7	-0.35 ± 0.26	-2.67 ± 0.71	0.62 ± 0.15
7588	1.216	2.176	91.72 ± 8.32	1.25 ± 0.7	-2.31 ± 0.12	0.88 ± 0.13
7588	2.176	3.136	78.56 ± 6.22	0.53 ± 0.58	-2.2 ± 0.13	1.12 ± 0.14
7588	3.136	4.224	67.31 ± 4.19	0.82 ± 0.68	-2.71 ± 0.13	0.63 ± 0.07
7588	4.224	5.44	62.78 ± 3.72	1.47 ± 0.89	-2.82 ± 0.14	0.48 ± 0.05
7588	5.44	6.72	56.13 ± 4.62	1.02 ± 1.16	-2.61 ± 0.12	0.5 ± 0.07
7588	6.72	8.384	54.95 ± 3.43	1.47 ± 1.23	-2.98 ± 0.18	0.29 ± 0.03

TABLE 2—*Continued*

Trigger#	t_{start} (s)	t_{end} (s)	E_p (keV)	α	β	flux (10^{-6} erg/cm 2 s)
7711	0.032	1.088	485 ± 74.7	-0.4 ± 0.13	-2.68 ± 0.46	1.85 ± 0.37
7711	1.088	1.856	261.9 ± 25.1	0.06 ± 0.18	-2.21 ± 0.23	2.35 ± 0.32
7711	1.856	2.624	213.4 ± 18.1	-0.15 ± 0.17	-2.04 ± 0.29	2.62 ± 0.34
7711	2.624	3.456	174 ± 16.5	-0.4 ± 0.18	-2.42 ± 0.22	1.48 ± 0.21
7711	3.456	4.48	128.2 ± 9.26	-0.38 ± 0.21	-2.79 ± 0.32	0.82 ± 0.1
7711	4.48	5.824	100.9 ± 7.57	-0.49 ± 0.28	-2.75 ± 0.27	0.58 ± 0.07
7711	5.824	7.808	64.81 ± 5.24	0.01 ± 0.73	-2.71 ± 0.18	0.33 ± 0.05
7711	7.808	13.76	48.74 ± 3.23	0.68 ± 1.42	-3.02 ± 0.21	0.13 ± 0.02
7711	13.76	28.672	31.95 ± 18.3	0.16 ± 11.7	-2.82 ± 0.31	0.04 ± 0.06